

Killing activity of neutrophils is mediated through activation of proteases by K^+ flux

Emer P. Reeves^{*†}, Hui Lu^{*†}, Hugues Lortat Jacobs[‡], Carlo G. M. Messina^{*}, Steve Bolsover[§], Giorgio Gabella^{||}, Eric O. Potma[¶], Alice Warley[#], Jürgen Roes[✉] & Anthony W. Segal^{*}

^{*}Centre for Molecular Medicine, Departments of § Physiology and || Anatomy and [✉] Windeyer Institute of Medical Sciences, University College London, 5 University Street, London WC1E 6JJ, UK

[‡]Institut de Biologie Structurale, 41 rue Horowitz, 38027 Grenoble, France

[¶]Ultrafast Laser and Spectroscopy Laboratory, Materials Science Centre, University of Groningen, Nijenborgh 4, 9747 AG Groningen, The Netherlands

[#]Rayne Institute, St Thomas' Hospital, Lambeth Palace Road, London SE1 7EH, UK

[†]These authors contributed equally to this work.

According to the hitherto accepted view, neutrophils kill ingested microorganisms by subjecting them to high concentrations of highly toxic reactive oxygen species (ROS) and bringing about myeloperoxidase-catalysed halogenation. We show here that this simple scheme, which for many years has served as a satisfactory working hypothesis, is inadequate. We find that mice made deficient in neutrophil-granule proteases but normal in respect of superoxide production and iodinating capacity, are unable to resist staphylococcal and candidal infections. We also show that activation provokes the influx of an enormous concentration of ROS into the endocytic vacuole. The resulting accumulation of anionic charge is compensated for by a surge of K^+ ions that cross the membrane in a pH-dependent manner. The consequent rise in ionic strength engenders the release of cationic granule proteins, including elastase and cathepsin G, from the anionic sulphated proteoglycan matrix. We show that it is the proteases, thus activated, that are primarily responsible for the destruction of the bacteria.

Metchnikoff discovered that 'phagocytes' confer immunity by engulfing invading microbes¹. It was supposed that killing was effected by the contents of the cytoplasmic granules released into the phagocytic vacuoles in which the microbes were encapsulated. This hypothesis was supplanted^{2,3} by the supposition that the killing agents were ROS^{4,5}, supported by the discovery of chronic granulomatous disease (CGD), a human condition characterized by profound susceptibility to bacterial and fungal infection⁶. The finding that phagocytes from these individuals are unable to generate ROS⁶ or to kill microbes efficiently was taken to imply that the respiratory burst promotes killing by generating toxic superoxide^{4,5} and H_2O_2 (ref. 7). The H_2O_2 was thought also to exert an indirect effect, as substrate for myeloperoxidase (MPO)-catalysed halogenation⁷.

According to this prevailing ROS model, a lack of proteases should not affect the killing ability of neutrophils. Although earlier studies had shown a requirement for neutrophil elastase to kill some Gram-negative bacilli⁸, and for both cathepsin G and elastase to protect against infection by *Aspergillus fumigatus*⁹, we extended these observations to microbes—*Staphylococcus aureus*¹⁰, the commonest cause of infection in CGD⁶, and *Candida albicans*—that, it was thought, could be killed only with the intervention of oxygen-dependent processes, because mice lacking MPO are abnormally sensitive to this pathogen¹¹.

Infections in protease-deficient mice

Figure 1 shows the results of intravenous injections of *S. aureus* (Fig. 1a) or *C. albicans* (Fig. 1b) on the survival of protease-deficient mice and *S. aureus* on CGD mice. Both organisms were much more virulent in the mice lacking both cathepsin G and elastase. A striking feature was the differential sensitivity of the two species of microbe to the two proteases. Cathepsin-G-deficient mice resisted *C. albicans* but not *S. aureus*, whereas the reverse was true for those lacking elastase (see also Supplementary Information).

The microbicidal activity of purified neutrophils determined *in vitro* (Fig. 1c, d) was the mirror image of the susceptibility *in vivo* (Fig. 1a, b). Under the same experimental conditions—microbial iodination—a composite measure of phagocytosis,

degranulation, oxidase activity and MPO activity was normal in these mice (Fig. 1f).

The addition of a cocktail of protease inhibitors to a suspension of human cells and bacteria also severely impaired killing (Fig. 1e); as expected, killing was also greatly reduced in CGD cells or those treated with the oxidase inhibitor diphenylene iodonium (DPI)¹².

Conditions within the phagocytic vacuole

ROS and protease deficiencies lead to comparable reductions in killing efficiency, implying that they act together on the internalized microbe. To clarify the nature of their interaction we set out to define conditions prevailing in the vacuole immediately after phagocytosis, when killing occurs¹³.

To estimate vacuolar volume, cross-sectional areas of phagocytic vacuoles were determined from electron micrographs, which indicated that the volume of the vacuole during the respiratory burst is about $0.2 \mu\text{m}^3$ (see Fig. 4a, b). For each molecule of O_2 consumed 4 superoxide (O_2^-) ions are generated (Fig. 2f). Between 0.2 (ref. 14) and 0.5 fmol (this study) of oxygen is consumed for each bacterium engulfed, resulting in an intravacuolar O_2^- release of about 4 mol l^{-1} . The steady-state concentrations of O_2^- and H_2O_2 attained are uncertain but have been surmised to be in the micromolar range¹⁵.

The large amounts of O_2^- , and therefore of its products, generated in the vacuole lead to the consideration that it might exert electrostatic or other physical effects, rather than merely providing the substrate for MPO. This conjecture was strengthened by observations on the cells of patients with incomplete CGD, or 'variant CGD'¹⁶, which still display impaired microbicidal activity despite generating about $0.5 \text{ mol l}^{-1} O_2^-$ in the vacuole. We accordingly examined phagocytic vacuoles by electron microscopy to search for evidence of oxidase-dependent changes in morphology. The vacuoles of normal cells were strikingly different in appearance from those of a patient with X-linked CGD (X-CGD), and another suffering from variant X-CGD with 12% oxidase activity (Fig. 2a–c). The granule contents were uniformly dispersed throughout the normal vacuoles but remained clumped in most of the CGD vacuoles and in those treated with DPI (not shown).

Knowing the vacuolar volume we determined the concentration of granule protein that entered vacuoles (Fig. 2d) as being about 0.5 g ml^{-1} . The pH in the vacuole rises from about 6.0 to 7.8–8.0 soon after phagocytosis, in consequence of oxidase activity^{13,17}, despite the entry of acid granule contents¹⁸. The O_2^- is released into the vacuole together with the granule contents, which exert a pH-buffering effect. This buffer capacity was estimated from the titre of KOH required to raise the pH from 5.5, at which the granules are maintained in the intact cell¹⁸, to a final value of 8.0 (Fig. 2e)¹³. This proved to be about $400 \mu\text{mol KOH}$ per gram of granule protein.

Oxidase pumps K^+ into the vacuole

We show here that the oxidase disperses the granules by pumping large amounts of K^+ into the vacuole.

The passage of electrons across the vacuolar membrane is

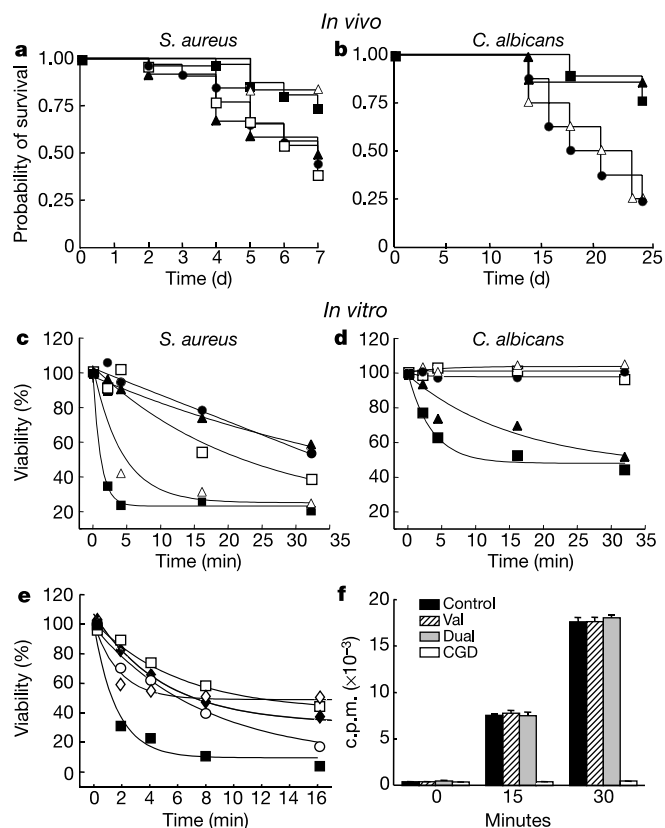


Figure 1 Susceptibility of protease-deficient mice to bacterial and fungal infection. **a, b**, Survival probability plots (Kaplan–Meier) of wild-type mice (filled squares, $n = 32$), or mice deficient in neutrophil elastase⁹ (open triangles, $n = 12$), cathepsin G⁹ (filled triangles, $n = 12$), elastase and cathepsin G⁹ (filled circles, $n = 31$) or p47^{phox} (ref. 9) (open squares, $n = 24$), injected intravenously with 4×10^7 *S. aureus* cells (**a**) or 10^4 *C. albicans* cells (**b**) (filled squares, $n = 9$; open triangles, $n = 8$; filled triangles, $n = 7$; filled circles, $n = 8$). The rates of decreased probability of survival for all mice were significantly different ($P < 0.05$) from wild type except for elastase-deficient (**a**) and cathepsin-G-deficient (**b**) animals, for which $P = 0.1$. **c, d**, Killing of *S. aureus* (**c**) and *C. albicans* (**d**) by mouse neutrophils (symbols as in **a**) *in vitro*. Killing rates for all mice were significantly different from wild type ($P < 0.01$) except for elastase-deficient (**c**) and cathepsin-G-deficient (**d**) cells ($P = 0.4$ and 0.9 , respectively). **e**, Killing of *S. aureus* by human neutrophils *in vitro* to show effects of addition of valinomycin (open circles), DPI (open diamonds) and protease inhibitors (filled diamonds). All compounds inhibited killing to the level seen with CGD cells (open squares) when compared with control cells (filled squares) ($P < 0.005$) and had no effect on bacteria. **f**, Time course of iodination by neutrophils from wild-type mice, mice deficient in cathepsin G and elastase (Dual) and mice deficient in p47^{phox} (CGD) exposed to *S. aureus*. The effect of the addition of valinomycin to normal cells is also shown (Val).

electrogenic¹⁹. The required charge compensation is commonly thought to be encompassed solely by the transfer of protons into the vacuole^{19–21} (Fig. 2f). Compensation of an electron by a proton is pH-neutral and cannot explain the observed elevation in vacuolar pH (ref. 13) that occurs despite the entry of acidic granule proteins into the vacuole. Cl^- ions could migrate from the vacuole to the cytosol, but the concentrations of 150 mM taken into the vacuole from the extracellular medium would not suffice to bring about

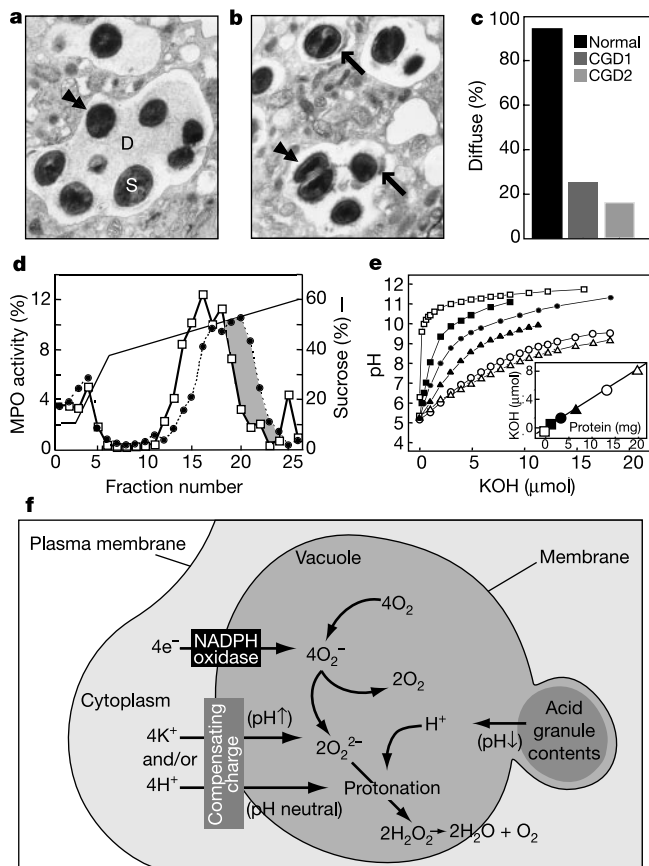


Figure 2 Appearance, concentration and buffering capacity of granule contents in the phagocytic vacuole. **a, b**, Granule contents within the vacuole (**a**) were classified as diffuse, because of their homogenous distribution (D), or clumped (arrows in **b**). Bacteria are indicated by double arrowheads. **c**, The proportion of vacuoles with a diffuse appearance in normal neutrophils ($n = 280$) and those from patients with X-linked CGD with complete absence of oxidase activity (CGD1, $n = 244$) or a variant patient with 12% oxidase activity (CGD2, $n = 206$) ($P = 10^{-148}$ and 10^{-68} between normal and X-CGD and between normal and variant X-CGD patients, respectively, by χ^2 analysis). **d**, Movement of granular proteins to the vacuole during phagocytosis of *S. aureus*. Distribution of MPO in phagocytosing (filled circles) compared with resting (open squares) neutrophils. Shading indicates movement of MPO to dense vacuoles containing bacteria. MPO composed 26% of the total granule protein. The protein content of 10^7 cells was 1.2 mg , of which $9.4 \pm 1.0\%$ (mean \pm s.e.m., $n = 4$) was in the granule fraction; 24%, or $\sim 0.1 \text{ pg}$ per vacuole, migrated to the vacuoles after the phagocytosis of 25 bacteria per cell. **e**, Buffering capacity of granule proteins (1 ml) at various concentrations titrated against KOH. Inset, amount of KOH required to elevate the pH from 5.5 to 8.0 for different amounts of protein. **f**, Schematic representation of factors involved in compensation of charge across the phagosomal membrane. The pH in the vacuole rises¹³, despite the influx of acidic granule contents, because of the consumption of H^+ within this compartment by the protonation of O_2^- and O_2^{2-} . If all the charge produced by pumping electrons across the phagosomal membrane were compensated by H^+ ions from the cytosol, the pH in the vacuole would not rise. We show here that part of the charge is compensated for by K^+ , which elevates the pH in a regulated manner and causes the vacuole to become hypertonic.

charge compensation. Cl^- has, in any case, been shown to move in the opposite direction in stimulated cells²². The rectifying movement of cations, in particular K^+ , from the cytoplasm where its concentration is high, into the vacuole, provides an alternative mechanism. First we studied the effect of valinomycin, a specific K^+ ionophore, on O_2^- production and O_2 consumption, and also that of 4-aminopyridine, a nonspecific K^+ -channel blocker²³ (Fig. 3a); both processes were markedly accelerated by the former and inhibited (albeit to a smaller extent) by the latter.

Because there is no known indicator of the required specificity and sensitivity for the measurement of K^+ at the high levels predicted in the vacuole, we determined its release into the medium after stimulation with the PKC agonist, 12-*O*-tetradecanoylphorbol-13-acetate (TPA), a potent activator of the oxidase. In response to this agent, which induces the oxidase to secrete O_2^- across the plasma membrane to the exterior, K^+ was released

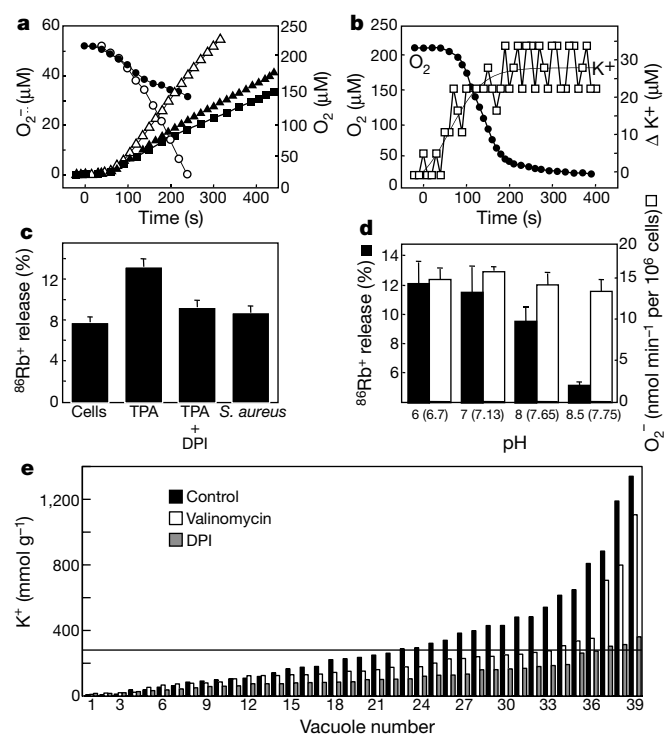


Figure 3 K^+ and ^{86}Rb transport associated with the generation of O_2^- in neutrophils. **a**, The rate of O_2^- release from 10^6 ml^{-1} cells is stimulated by valinomycin ($3 \mu\text{M}$, 3 min; open triangles) and inhibited by 4-aminopyridine (4 mM , 3 min; filled squares) compared with control cells (filled triangles) (representative of three experiments) in response to TPA (10 ng ml^{-1}). O_2 consumption by 10^7 cells phagocytosing *S. aureus* in the absence (filled circles) and the presence (open circles) of valinomycin is also shown. **b**, Time course of release of K^+ into medium (open squares) in relation to oxygen consumption (filled circles) after stimulation of 4×10^7 cells ml^{-1} with TPA ($1 \mu\text{g ml}^{-1}$). **c**, $^{86}\text{Rb}^+$ release from 10^7 cells before (Cells) or after stimulation with TPA ($1 \mu\text{g ml}^{-1}$), or phagocytosis of *S. aureus*. Oxygen consumption was equivalent after these stimuli and was inhibited by DPI. **d**, $^{86}\text{Rb}^+$ release (black columns), but not O_2^- generation (white columns), was inhibited by elevating the pH to 8 or more. The pH values of the external buffer and of cytosol (in parentheses) are shown. (All results are means \pm s.e.m. from at least three measurements). **e**, K^+ concentrations in phagocytic vacuoles of neutrophils after the phagocytosis of *S. aureus*, and the effects on this of the addition of valinomycin and DPI, as determined by electron probe X-ray microanalysis. The horizontal line depicts the mean concentration (280 mmol g^{-1}) in control cytosol. (Median, mean, *n* and s.e.m. of values in vacuoles were: 236, 322, 39 and 50; 152, 213, 39 and 34; and 100, 121, 39 and 13 mmol g^{-1} for cells treated with control, valinomycin and DPI, respectively. The corresponding values in cytosols were 291, 280, 41 and 22; 211, 269, 46 and 38; and 278, 345, 37 and 46.)

into the medium, and this was blocked by DPI (Fig. 3b). Measurements with the K^+ electrode were only semiquantitative, so $^{86}\text{Rb}^+$, commonly used as a marker of K^+ in transport studies²⁴, was used for quantification. Secretion of this ion was suppressed by DPI (Fig. 3c) and is thus contingent upon O_2^- generation rather than on PKC activation by the phorbol ester. To show that this release was spatially coupled to the O_2^- -generating machinery and not to general leakage from respiring cells, we measured secretion in conditions favouring the flux of K^+ , Rb^+ or O_2^- into the closed phagocytic vacuole²⁵ encapsulating an engulfed bacterium. In these circumstances, release to the exterior was not observed, even though an equivalent amount of oxygen was consumed.

We used electron-probe X-ray microanalysis to obtain a direct estimate of the K^+ content of the phagosome (Fig. 3e). In DPI-treated cells the vacuolar K^+ concentration was much less than that in untreated control cells (mean \pm s.e.m. $122 \pm 15 \text{ mmol g}^{-1}$ ($n = 35$) and $314 \pm 22 \text{ mmol g}^{-1}$ ($n = 40$), respectively; $P < 0.001$ by Wilcoxon rank-sum), clearly implicating the oxidase in the accumulation of K^+ in this compartment. A wide range of values is measured in normal vacuoles in consequence of the asynchronous nature of phagocytosis. To take into account the wide spread of results obtained with the microprobe technique, and to detect a skewing of the distribution towards higher concentrations, we compared the upper quartiles of K^+ measurements in the vacuoles with those in the corresponding cytosol. We found them to be significantly higher in the control cells ($P < 0.03$ by Wilcoxon rank-sum), no different in the valinomycin-treated cells ($P = 0.16$) and much lower in cells exposed to DPI ($P = 0.0003$). Microprobe analysis gave a median concentration of K^+ of 290 mmol g^{-1} in the cytosol of normal cells, which we take to correspond to the experimentally measured concentration of 125 mM (ref. 27). This ratio leads to a value of 270 mM for the upper quartile in normal vacuoles, corresponding to the microprobe measurement of 631 mmol g^{-1} . Thus we can conclude that K^+ concentrations in the range 200–300 mM are attained in the vacuole (see also Supplementary Information).

What sets the level of charge compensation by K^+ ? Each molecule of O_2^- generates one OH^- ion. If all the charge were to be compensated for by K^+ the OH^- would overwhelm the buffering capacity of the granules and the pH would be excessively elevated. The regulation of the proportion of compensating charge made up by K^+ seems to depend on the pH itself. The efflux of $^{86}\text{Rb}^+$ to the exterior after stimulation with TPA was reduced when the pH of the medium was elevated to 8.0, and almost eliminated at pH 8.5, even though O_2^- production was virtually unchanged at the higher pH (Fig. 3d). At high pH the charge is likely to be compensated for almost entirely by H^+ . In this way the amount of K^+ entering the vacuole could be linked to degranulation. The more granule contents are released into the vacuole, the more the pH is depressed and the greater the buffering capacity. A parallel increase in the proportion of the charge compensated for by K^+ would be required for transport of this ion to be impeded by a rise in pH.

K^+ influx renders the vacuole hypertonic

After a lag of about 1 min after stimulation, 10^7 neutrophils produce approximately 300 nmol of O_2^- in the ensuing 2 min (Fig. 3a, b). With a cellular volume of $345 \mu\text{m}^3$ and a K^+ concentration of 125 mM (ref. 26), 2.9×10^9 cells occupy 1 ml and contain $125 \mu\text{mol}$ of K^+ , of which, judging from the $^{86}\text{Rb}^+$ measurement, roughly 4.5%, or $5.6 \mu\text{mol}$, would be released. Over the same interval the cells would produce about $90 \mu\text{mol}$ of O_2^- , a molar ratio to K^+ secretion of approximately 16:1. The release of 4 mol l^{-1} O_2^- in the vacuole then leads to the expected intravacuolar K^+ concentration in the range 200–300 mM, very similar to that measured by X-ray microanalysis. One electron charge compensated by K^+ generates one OH^- , so the levels of OH^- that would be produced agree satisfactorily with the alkali titre required to raise

the pH in the presence of the predicted concentration of granule contents.

Tonicity in the vacuole must initially be high. The K^+ driven into the vacuole by the burst is added to the 150 mM NaCl, incorporated from the extracellular medium when the vacuole forms. Dilution of these salts occurs only later, as swelling of the vacuoles¹³ (Fig. 4a, b) sets in well after the end of the respiratory burst. To understand why swelling does not ensue immediately, we first used coherent anti-Stokes Raman scattering (CARS) laser-scanning microscopy²⁷ to determine whether the vacuolar membrane was unusually impermeable to water. The results showed the membrane surrounding the vacuole to be permeable to H_2O (Fig. 4c–e), with a permeability constant of $6 \mu m s^{-1}$ or higher, roughly similar to that of the plasma membrane of *Dictyostelium discoideum* cells²⁷; thus another explanation is required for the delay in swelling. It turns out that the vacuole is constrained by a surrounding meshwork of cytoskeletal proteins, as seen in macrophages³⁸, including vinculin and paxillin. These proteins initially accumulate around the vacuole and then slowly disperse as swelling proceeds (Fig. 4f, g). When the membrane-permeant fungal toxin jasplakinolide²⁹ was used to stabilize filamentous actin, swelling of the vacuoles was prevented (Fig. 4b).

Because valinomycin has such a profound effect in suppressing bacterial killing and vacuolar swelling, despite occasioning a marked enhancement of the respiratory burst, we measured its effect on vacuolar pH. We found that valinomycin caused a large decrease in vacuolar pH (Fig. 5e), to the low values observed in cells lacking the oxidase activity, either because of CGD¹³ or inhibition by DPI¹². A possible explanation for this effect is that almost twice as much oxygen is consumed for each bacterium engulfed in valinomycin-treated cells, and thus more cations are required for charge compensation. K^+ ions are lost from the vacuole through the valinomycin channel, so that the charge must be compensated for by the passage of protons, with consequent acidification. The pH in

the vacuoles of the valinomycin-treated cells is below the optimum for both elastase and cathepsin G (Fig. 5f), a contributing factor to the impairments of killing (Fig. 1e) and digestion (Fig. 5d) induced by the ionophore.

With regard to the force within the vacuole responsible for swelling, the osmotic effect of the added K^+ is in itself probably insufficient. Fairly high levels of K^+ were measured in the presence of valinomycin, yet there was no swelling; protease inhibitors, which should not perturb K^+ fluxes, also prevented swelling (Fig. 4b). Swelling seems instead to be linked to the digestion of vacuolar contents and thus probably results from the osmotic pressure exerted by the products of this process. Digestion and swelling are both impaired in the absence of the oxidase, either naturally in CGD¹³ or after inhibition by DPI, by valinomycin or by protease inhibitors (Fig. 5d), or when microbes are replaced by protease-resistant latex particles¹³. The osmotic forces in the vacuole must be considerable as they cause the ingested bacteria to shrink to about half their original volume (Fig. 4a inset, b) before partly recovering as the vacuoles swell.

Hypertonicity activates granule proteases

How then might the K^+ enter into the killing process? Clearly it can do so by enabling the pH in the vacuole to rise as it substitutes for H^+ in compensating for the potential difference across the membrane generated by the oxidase. However, it also exerts a quite separate effect by activating the granule enzymes. The granules contain a strongly anionic sulphated proteoglycan matrix to which the cationic proteases are tightly bound³⁰. A model for this is the affinity of some of these proteases for heparin as shown by surface plasmon resonance in Fig. 5a. In this bound state they cannot reach the ingested microbe and must be solubilized to become functional. We propose that this activation is brought about by the hypertonic K^+ , driven into the vacuole by the NADPH oxidase. Figure 5b shows that most of the granule protein is solubilized at the K^+ concentrations

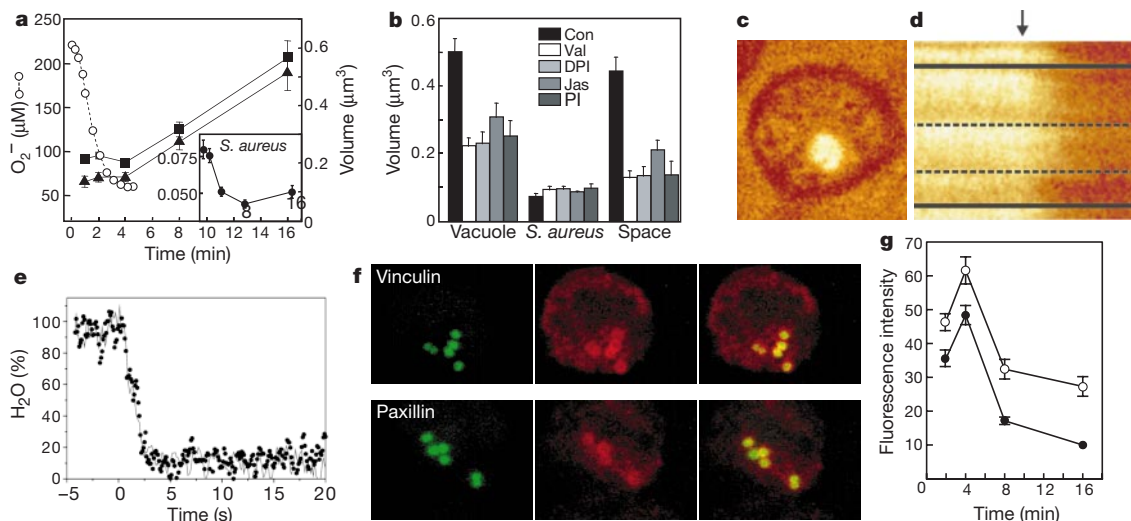


Figure 4 Vacuolar swelling and its control. **a**, Time course of the changes in the volume of the phagocytic vacuole (filled squares), the enclosed bacterium (filled circles, insert) and the intervening space (filled triangles) determined by electron microscopy on 24, 43, 65, 45 and 24 vacuoles measured after 1, 2, 4, 8 and 16 min respectively. The bacteria re-swelled significantly between 8 and 16 min ($P < 0.05$ by Student's t -test). The time course of oxygen consumption is also shown (open circles). **b**, The effect on the size of the vacuoles of exposing cells to valinomycin (Val, $3 \mu M$, $n = 106$), DPI ($5 \mu M$, $n = 44$), jasplakinolide ($1 \mu M$, $n = 74$) and protease inhibitors (PI, $n = 30$) compared with untreated cells (Con, $n = 111$) at 16 min after phagocytosis. All additions resulted in highly significant differences ($P < 0.001$) from control cells. **c**, CARS image of neutrophil with superimposed fluorescence image of ANTS-labelled, phagocytosed *C. albicans*. **d**, Real-

time permeability experiment showing the CARS signal from water on the left and the ensuing decrease in signal after rapid exchange (arrow) of aqueous medium against isotonic 2H_2O buffer. Solid lines mark the plasma membrane of the cell and dashed lines indicate the edges of the intracellular vacuole. **e**, Dynamics of water efflux from the vacuole upon rapid $H_2O/^2H_2O$ exchange. Dots refer to experimental data points. The solid line fitted to the data reveals an efflux time of H_2O from the vacuole of ~ 0.1 s. **f**, Fluorescein-labelled *S. aureus* (approximate diameter $0.8 \mu m$) in phagocytic vacuoles (green, left panels) of neutrophils stained for vinculin or paxillin (red, middle panels). These cytoskeletal proteins surround the vacuole (composite images, right panels). **g**, Amounts of vinculin (open circles) and paxillin (filled circles) around the vacuole diminish with time as swelling occurs (each point is the mean of 50 measurements).

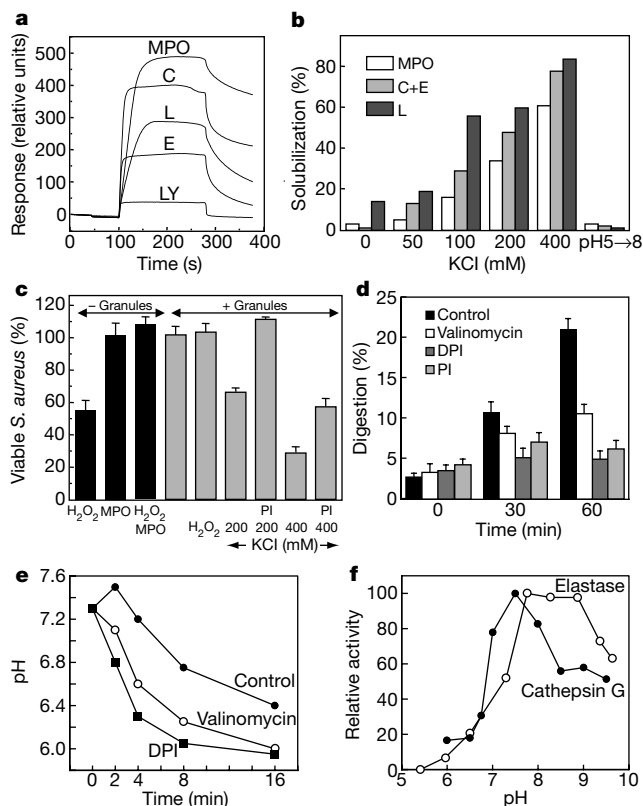


Figure 5 Activation of the microbicidal proteases requires K^+ and neutral pH. **a**, The cationic granule proteins bind strongly to proteoglycans. Surface plasmon resonance plots of binding of pure MPO (K_d 20.4 nM), cathepsin G (C, K_d 5.3 nM), lactoferrin (L, K_d 28.3 nM) and elastase (E, K_d 8.9 nM) to heparin. Lysozyme (LY) did not bind significantly. All proteins were present at $4 \mu\text{g ml}^{-1}$. **b**, MPO, cathepsin G and elastase (C+E) and lactoferrin (L) were released from the granule matrix at elevated salt concentrations but not by increasing the pH from 5 to 8 (granules 20 mg ml^{-1}). **c**, The effect of H_2O_2 (100 mM), alone or with MPO (5 mg ml^{-1}), and purified neutrophil granules (44 mg ml^{-1}), in the presence and absence of KCl and/or protease inhibitors (PI) on the viability of *S. aureus*. All results are means \pm s.e.m. from at least three measurements. **d**, Effect of valinomycin, DPI and protease inhibitors (PI) on digestion of ^{35}S -labelled, killed, *S. aureus*. **e**, Effect of DPI and valinomycin on vacuolar pH over time. Each point is the mean of at least three measurements with fluorescein-coated bacteria as pH indicators^{13,17}. pH values at 2 min were significantly different ($P < 0.05$ by Student's *t*-test). **f**, Relation between pH and activity of cathepsin G and elastase. Each point is the mean of three measurements.

achieved in the vacuole. Elevated pH on its own was without effect. Isolated granules were not bactericidal but became so at higher KCl concentrations, an effect that was partly abrogated by protease inhibitors (Fig. 5c). The fact that some of the antimicrobial activity of the cationic proteins is independent of their enzymic function³¹ could account for this inhibitor-resistant killing. The concentrations of H_2O_2 developed in the vacuole are not known but it seems unlikely that they could exceed 100 mM, because at such high levels the catalase activity of MPO supervenes^{32,33}; the action of H_2O_2 on microbes was therefore measured at this concentration. Only limited microbicidal activity was recorded, and even this was suppressed completely by the addition of granules. MPO also inhibited killing, despite the presence in the medium of Cl^- , a substrate for chlorination reactions. Lower concentrations of H_2O_2 , down to 100 μM , also failed to kill, with or without MPO (not shown).

Discussion

Our results have uncovered a previously unsuspected mechanism of antimicrobial activity in the phagocyte. In brief, the O_2^- -generating

system causes an influx of K^+ into the phagocytic vacuole with an attendant rise in pH to the optimal level for the activity of the granule proteases. Moreover, these become active on release from the anionic proteoglycan matrix at the elevated ionic strength.

It is essential that the volume of the vacuole be restricted for the requisite hypertonicity to develop. This requires the integrity of the cytoskeletal network, and disruption of this by microbial products could offer a mechanism of virulence by inhibiting the activation of the granule proteins³⁴.

The identity and nature of the K^+ channel will be of interest; it might or might not be the well-studied H^+ channel. One suggestion has been that gp91^{phox}, the flavocytochrome *b* of the NADPH oxidase, is itself the channel^{35,36}, although contradictory evidence exists^{37,38}.

One might question the need for such an elaborate activation system. A possible explanation lies in the very large numbers of neutrophils that infiltrate sites of acute inflammation and the potential of their enzymes to damage autologous tissues if released from cells in a freely soluble, active, form. For example, the mouse lacking both cathepsin G and elastase is relatively resistant to endotoxin shock, in which damage to the endothelium by the endotoxin is followed by neutrophil attack; this implicates these two proteases in the tissue damage that normally occurs in this situation⁹. The hazard of injurious effects from these enzymes in normal tissues is reduced by packaging them in an inactive form adsorbed on acidic proteoglycans, from which they are released and activated only by a combination of the unusual conditions of hypertonicity and alkalinity prevailing in the phagocytic vacuole.

Our demonstration that ROS generation and MPO activity are not themselves sufficient to kill key model target organisms is important, not only because of the insight it affords into normal immunity, but also because of the light it throws on pathological mechanisms. Early theories implicating oxygen radicals in tissue damage³⁹ stemmed from the apparent toxicity of these agents against microbes, which are much tougher than human cells. Some of this early supportive evidence will need to be reassessed in the light of the above developments^{4,5}. Experiments with MPO were generally performed at what has been shown here to be unphysiologically low concentrations of enzyme and H_2O_2 and at too low a pH (ref. 7).

MPO still seems to be important in the killing process^{7,11}. It might help to protect the microbicidal enzymes against oxidative damage. In preliminary studies we have found cathepsin G to be very sensitive to oxidation by H_2O_2 and to be inactivated at a greatly increased rate in phagocytosing neutrophils treated with azide to inhibit MPO. Similar mechanisms of oxidative inactivation of degradative enzymes could explain the accelerated deposition of atheromatous material observed in MPO-deficient mice^{40,41}. □

Methods

Infection studies

Staphylococcus aureus (NCTC 12981) cells (4×10^7) or *C. albicans* cells (10^4) from an overnight culture were injected into the tail veins of mice deficient in cathepsin G and/or neutrophil elastase, CGD mice deficient in p47^{phox} or normal mice, all on the strain 129 genetic background⁹. Survival was monitored every 12 h for 7 d (*S. aureus*) and 24 d (*C. albicans*), respectively.

Measurements of neutrophil function in vitro

Neutrophils were purified from human blood¹³ and suspended in PBS (140 mM NaCl, 10 mM KCl, 10 mM NaH_2PO_4 , 5 mM glucose, pH 7.3). All mixing of microbes with neutrophils *in vitro* was done in the rapidly stirred chamber of an oxygen electrode at 37 °C. All additions of chemicals to cell suspensions were made without subsequent incubation unless stated otherwise.

Thioglycollate-elicited mouse neutrophils (2.8×10^7) (ref. 9) in 0.5 ml were mixed with 5×10^6 *S. aureus* or 2.5×10^6 *C. albicans* cells. Killing was measured as described¹³, omitting lysostaphin. All killing studies *in vitro* were performed in duplicate with cells from three to five mice, and colonies were counted on three aliquots taken at each time point.

Iodination by mouse neutrophils was measured on cells purified from thioglycollate (3%)–induced peritoneal exudates and with the use of immune mouse serum as opsonin⁴². Results of three experiments with three measurements in each are shown in Fig. 1f.

To measure the effect of valinomycin (3 μM), DPI (5 μM) or protease inhibitors (10 $\mu\text{g ml}^{-1}$ leupeptin, *N*-tosyl-L-leucine chloromethyl ketone (TLCK), pepstatin A, aprotinin and diisopropylfluorophosphate 1 mM) on killing by human neutrophils, 10⁸ cells in 1 ml PBS were mixed with 10⁸ IgG-opsonized *S. aureus*, in the presence and in the absence of valinomycin or protease inhibitors, and then treated as above. To study the effect of jasplakinolide (1 μM) without inhibiting phagocytosis, cells were mixed with bacteria for 2 min; the agent was then added and cells were incubated at 37 °C for a further 14 min.

O₂⁻ generation was determined by superoxide-dismutase-inhibitable reduction of cytochrome *c*⁴ and oxygen consumption with an oxygen electrode¹⁴. Digestion of heat-killed (65 °C, 30 min) ³⁵S-methionine-labelled *S. aureus* cells was expressed as the percentage of trichloroacetic-acid (10%) -soluble radioactivity released into the supernatant¹³.

Survival analysis

Survival of mice was analysed by Kaplan–Meier survival analysis. Killing *in vitro* was analysed by determining the rate of loss of viability of the organisms by regression analysis of a logarithmic transformation of the numbers of surviving microbes in relation to time. Slopes were compared with a two-tailed *t*-test.

Electron and confocal microscopy

To assess the sizes of phagocytic vacuoles and their contents, 5 × 10⁷ fresh human neutrophils were mixed with 5 × 10⁸ IgG-opsonized *S. aureus* cells in a rapidly stirred chamber at 37 °C. At timed intervals, aliquots were taken into a fixative consisting of glutaraldehyde (1.5%), picric acid (0.1%) in sodium cacodylate buffer (0.1 M, pH 7.2). They were postfixed in osmium tetroxide, dehydrated in ethanol and embedded in Araldite. Sections were collected on copper grids, contrast-stained with uranyl acetate and lead citrate and viewed at a magnification of ×16,000. Morphometry was performed by projecting the photographic electron-microscopy negatives through a microfilm reader, giving a further enlargement of ×9 or ×12. The relevant structures (and the calibration bars) were traced on paper and the profiles were then measured with a digitizing tablet. Only the volumes of phagocytic vacuoles that were judged to have been sectioned in the region of maximum width were measured.

For assessment of the dispersion of granule contents in the vacuole, the cells were treated as above and the incubation was ended at 4 min. Granule contents in the vacuoles were visually assessed as dispersed or not by two independent 'blinded' observers.

Immunohistochemical analysis of phagocytosing neutrophils was conducted as described previously¹⁵ with antibodies against paxillin and vinculin (from Santa Cruz). The fluorescence intensity around 50 vacuoles was measured at each time point and compared with that in the surrounding cytosol by using a Leica TCS NT confocal microscope.

Measurement of K⁺ and ⁸⁶Rb⁺ fluxes

K⁺ release from neutrophils (4 × 10⁷ ml⁻¹) stimulated with 1 $\mu\text{g ml}^{-1}$ TPA was measured continuously with a K⁺ electrode (Thermo Russell, Model 93-3199) at 37 °C. The cells were kept in PBS and the buffer was exchanged to a K⁺-free PBS just before each measurement. K⁺ efflux was measured in the absence and in the presence of 5 μM DPI. K⁺ concentration was calculated from a standard curve.

For ⁸⁶Rb⁺ efflux, 10⁷ neutrophils were suspended in 1 ml 136 mM NaCl, 1 mM MgSO₄, 1 mM CaCl₂, 5 mM KCl, 5.6 mM glucose, 20 mM HEPES pH 7.4 (HEPES buffer), 2.5 μCi ⁸⁶Rb⁺ and 0.1 mg ml⁻¹ bovine serum albumin (BSA) and incubated at 30 °C for 30 min, washed three times in the buffer without the ⁸⁶Rb⁺ and then placed in a stirred oxygenated chamber at 37 °C. Cells were stimulated with either 2 × 10⁸ IgG-opsonized *S. aureus* or 1 $\mu\text{g ml}^{-1}$ TPA for 3.5 min. Stimulated cells were immediately cooled to 4 °C and centrifuged through Ficoll/Hypaque at 400g for 10 min at 4 °C. Radioactivity in the supernatant above the Ficoll/Hypaque and in the neutrophil pellet was removed and counted in a liquid-scintillation counter. ⁸⁶Rb⁺ efflux was also measured in 20 mM HEPES buffer at pH 6, 7, 8 and 8.5.

K⁺ concentrations inside the phagocytic vacuole and cytoplasm were measured by X-ray microanalysis on snap-frozen, freeze-dried cells. Neutrophils (with and without DPI or valinomycin) were mixed with IgG-opsonized *S. aureus* at 37 °C for 3 min and centrifuged at 800g for 10 s; drops of the thick cell pellet were collected on a piece of Millipore filter paper and cryofixed by being plunged into liquid propane. The cryofixed pellets were stored under liquid nitrogen. Cryosections 250 nm thick were cut at -120 °C in an RMC MTXL cryo-ultramicrotome. The sections were supported on Ploioform-covered nickel grids (100 mesh hexagonal) and freeze-dried overnight under temperature-controlled conditions. The sections were coated with a thin layer of carbon in the vacuum chamber and analysed with a Zeiss EM10 electron microscope fitted with an Oxford Instruments detector and PGT Avalon 8000 microanalysis system. Areas within the vacuole space and in the adjacent cytoplasm were analysed with a reduced-area raster for 60 s of live time at an accelerating voltage of 80 kV and an beam current of 1 nA in STEM mode at ambient temperature. Spectra were processed and quantification was achieved with the peak-to-continuum ratio method¹⁴. Results are expressed as mmol g⁻¹ dry weight.

Granule and protein purification, enzyme activity and plasmon resonance

Human buffy coat neutrophils were disrupted by nitrogen cavitation in Break buffer (10 mM KCl, 3 mM NaCl, 4 mM MgCl₂, 10 mM PIPES pH 7.2) containing protease inhibitors (leupeptin, TLCK and pepstatin A, each at 1 $\mu\text{g ml}^{-1}$). Post-nuclear supernatants (PNSs) were prepared by centrifugation at 400g at 4 °C for 10 min.

The PNS was centrifuged for 1 h at 100,000g in a Beckman SW41 head at 4 °C on discontinuous gradients of 33% sucrose on 55% sucrose (w/w), and the granules were

removed from the interface. Human MPO was purified from granules to a Reinheit Zahl (Rz) value (A₄₃₀/A₂₈₀) of 0.82 (ref. 45).

For purification of cathepsin G, neutrophil elastase, lactoferrin and lysozyme, the granules were homogenized in Break buffer and 1% cetyltrimethylammonium bromide. The extract was centrifuged at 25,000g for 10 min. The supernatant was loaded on a Fast Flow S-Sepharose column (1.5 cm × 20 cm) in 10 mM phosphate buffer pH 6.95 and eluted with a linear gradient of NaCl (10 mM to 1 M). Lysozyme, cathepsin G and lactoferrin were further purified on a Mono S column (1 ml) with the same buffer and salt gradient. Elastase was further purified on heparin–agarose in the same buffer and salt gradient followed by gel filtration on a Superdex 75 column (all resins from Pharmacia). All proteins were at least 95% pure and identities were confirmed by matrix-assisted laser desorption/ionization mass spectrometry. Protein binding to heparin was measured by surface plasmon resonance (Biacore) as described¹⁶.

To determine the quantity of granule proteins in the vacuole, bacteria were labelled with [³⁵S]methionine, heat-killed (70 °C for 10 min), opsonized with human IgG and mixed with cells at a ratio of 20:1 at 37 °C for 4 min. Unopsonized bacteria were used as a control. Phagocytosis was stopped by placing cells into ice-cold PBS in which they were washed twice and then lysed by nitrogen cavitation in Break buffer containing 11.2% (w/w) sucrose. The PNS was centrifuged into a 12-ml continuous sucrose gradient from 30% to 60% (w/w) at 150,000g for 2 h in a Beckman SW41 head. Fractions (0.5 ml) were counted for bacteria and assayed for MPO (with *o*-dianisidine) or protein (with Bradford reagent from Bio-Rad) with BSA as standard.

Membranes were removed from granules⁴⁷ by centrifugation through Percoll. To measure the buffering capacity of granule proteins, various concentrations of granules lacking membranes, suspended in normal saline, were titrated against KOH and the pH was measured.

The pH dependence of the activities of elastase and cathepsin G⁴⁸ (both from Sigma) was measured exactly as described.

Killing of *S. aureus* by granule proteins

Granules without membranes were prepared in the absence of protease inhibitors. Bacteria were incubated for 6 min with H₂O₂ (100 mM) in the presence or absence of MPO (5 mg ml⁻¹) or granules (44 mg ml⁻¹) in PBS at 37 °C. Granules were also incubated in the presence of KCl (200 or 400 mM), with or without protease inhibitors as above.

Measurement of vacuolar permeability to water

Purified neutrophils were left to adhere to poly-(L-lysine)-coated slides for 15 min at 37 °C. The slides were washed with PBS and then overlaid for 15 min with a suspension of *C. albicans* labelled with the fluorophore 8-aminonaphthalene-1,3,6-trisulphonic acid (ANTS; Molecular Probes) and opsonized with human IgG. Unattached *Candida* cells were washed away and nonlinear coherent CARS microscopy was performed, in combination with isotopic exchange, as described¹⁷.

Vacuolar and cytosolic pH

Vacuolar pH was determined from the excitation spectrum of fluorescein-labelled, IgG-coated *S. aureus*¹³ exactly as described¹⁷. Cytosolic pH was measured in cells in suspension with the fluorescent indicator 2',7'-bis-(carboxyethyl)-5(6)-carboxyfluorescein¹⁹, and pH values were standardized with phosphate-buffered or HEPES-buffered salt solutions; cells were equilibrated in the presence of either *p*-(trifluoromethoxy)phenylhydrazone (10 μM) or nigericin (10 μM).

Received 12 December 2001; accepted 23 January 2002.

1. Metchnikoff, B. *Immunity in Infective Diseases* (Cambridge Univ. Press, 1905).
2. Sbarra, A. J. & Karnovsky, M. L. The biochemical basis of phagocytosis. 1. Metabolic changes during the ingestion of particles by polymorphonuclear leukocytes. *J. Biol. Chem.* **234**, 1355–1362 (1959).
3. Mandell, G. L. Bactericidal activity of aerobic and anaerobic polymorphonuclear neutrophils. *Infect. Immun.* **9**, 337–341 (1974).
4. Babior, B. M., Curnutte, J. T. & Kipnes, R. S. Biological defense mechanisms. Evidence for the participation of superoxide in bacterial killing by xanthine oxidase. *J. Lab. Clin. Med.* **85**, 235–244 (1975).
5. Babior, B. M., Kipnes, R. S. & Curnutte, J. T. Biological defence mechanisms: the production by leukocytes of superoxide, a potential bactericidal agent. *J. Clin. Invest.* **52**, 741–744 (1973).
6. Thrasher, A. J., Keep, N. H., Wientjes, F. & Segal, A. W. Chronic granulomatous disease. *Biochim. Biophys. Acta* **1227**, 1–24 (1994).
7. Klebanoff, S. J. Antimicrobial mechanisms in neutrophilic polymorphonuclear leukocytes. *Semin. Hematol.* **12**, 117–142 (1975).
8. Belaouaj, A. *et al.* Mice lacking neutrophil elastase reveal impaired host defense against Gram-negative bacterial sepsis. *Nature Med.* **4**, 615–618 (1998).
9. Tkalecic, J. *et al.* Impaired immunity and enhanced resistance to endotoxin in the absence of neutrophil elastase and cathepsin G. *Immunity* **12**, 201–210 (2000).
10. Hampton, M. B., Kettle, A. J. & Winterbourn, C. C. Involvement of superoxide and myeloperoxidase in oxygen-dependent killing of *Staphylococcus aureus* by neutrophils. *Infect. Immun.* **64**, 3512–3517 (1996).
11. Aratani, Y., Koyama, H., Nyui, S., Suzuki, K., Kura, F. & Maeda, N. Severe impairment in early host defense against *Candida albicans* in mice deficient in myeloperoxidase. *Infect. Immun.* **67**, 1828–1836 (1999).
12. Cross, A. R. & Jones, O. T. The effect of the inhibitor diphenylene iodonium on the superoxide-generating system of neutrophils. Specific labelling of a component polypeptide of the oxidase. *Biochem. J.* **237**, 111–116 (1986).
13. Segal, A. W., Geisow, M., Garcia, R., Harper, A. & Miller, R. The respiratory burst of phagocytic cells is associated with a rise in vacuolar pH. *Nature* **290**, 406–409 (1981).

14. Segal, A. W. & Coade, S. B. Kinetics of oxygen consumption by phagocytosing human neutrophils. *Biochem. Biophys. Res. Commun.* **84**, 611–617 (1978).
15. Hampton, M. B., Kettle, A. J. & Winterbourn, C. C. Inside the neutrophil phagosome: oxidants, myeloperoxidase, and bacterial killing. *Blood* **92**, 3007–3017 (1998).
16. Bu-Ghanim, H. N., Segal, A. W., Keep, N. H. & Casimir, C. M. Molecular analysis in three cases of X91-variant chronic granulomatous disease. *Blood* **86**, 3575–3582 (1995).
17. Jiang, Q., Griffin, D. A., Barofsky, D. F. & Hurst, J. K. Intraphagosomal chlorination dynamics and yields determined using unique fluorescent bacterial mimics. *Chem. Res. Toxicol.* **10**, 1080–1089 (1997).
18. Styrts, B. & Klempner, M. S. Internal pH of human neutrophil lysosomes. *FEBS Lett.* **149**, 113–116 (1982).
19. Henderson, L. M., Chappell, J. B. & Jones, O. T. The superoxide-generating NADPH oxidase of human neutrophils is electrogenic and associated with an H⁺ channel. *Biochem. J.* **246**, 325–329 (1987).
20. Nanda, A. & Grinstein, S. Protein kinase C activates an H⁺ (equivalent) conductance in the plasma membrane of human neutrophils. *Proc. Natl Acad. Sci. USA* **88**, 10816–10820 (1991).
21. DeCoursey, T. E., Cherny, V. V., Zhou, W. & Thomas, L. L. Simultaneous activation of NADPH oxidase-related proton and electron currents in human neutrophils. *Proc. Natl Acad. Sci. USA* **97**, 6885–6889 (2000).
22. Menegazzi, R., Busetto, S., Dri, P., Cramer, R. & Patriarca, P. Chloride ion efflux regulates adherence, spreading, and respiratory burst of neutrophils stimulated by tumor necrosis factor- α (TNF) on biologic surfaces. *J. Cell Biol.* **135**, 511–522 (1996).
23. Clapp, L. H. & Tinker, A. Potassium channels in the vasculature. *Curr. Opin. Nephrol. Hypertens.* **7**, 91–98 (1998).
24. Love, W. D. & Burch, G. E. A comparison of potassium⁴², rubidium⁸⁶, and cesium¹³⁴ as tracers of potassium in the study of cation metabolism of human erythrocytes *in vitro*. *J. Lab. Clin. Med.* **41**, 351–362 (1953).
25. Segal, A. W. & Meshulam, T. Production of superoxide by neutrophils: a reappraisal. *FEBS Lett.* **100**, 27–32 (1979).
26. Ince, C. *et al.* Intracellular K⁺, Na⁺ and Cl⁻ concentrations and membrane potential in human monocytes. *Biochim. Biophys. Acta* **905**, 195–204 (1987).
27. Potma, E., de Boeij, W. P., van Haastert, P. J. & Wiersma, D. A. Real-time visualization hydrodynamics in single living cells. *Proc. Natl Acad. Sci. USA* **98**, 1577–1582 (2001).
28. Aderem, A. & Underhill, D. M. Mechanisms of phagocytosis in macrophages. *Annu. Rev. Immunol.* **17**, 593–623 (1999).
29. Rizoli, S. B., Rotstein, O. D., Parodo, J., Phillips, M. J. & Kapus, A. Hypertonic inhibition of exocytosis in neutrophils: central role for osmotic actin skeleton remodeling. *Am. J. Physiol. Cell Physiol.* **279**, C619–C633 (2000).
30. Kolset, S. O. & Gallagher, J. T. Proteoglycans in haemopoietic cells. *Biochim. Biophys. Acta* **1032**, 191–211 (1990).
31. Odeberg, H. & Olsson, I. Antibacterial activity of cationic proteins from human granulocytes. *J. Clin. Invest.* **56**, 1118–1124 (1975).
32. Winterbourn, C. C., Garcia, R. C. & Segal, A. W. Production of the superoxide adduct of myeloperoxidase (compound III) by stimulated human neutrophils and its reactivity with hydrogen peroxide and chloride. *Biochem. J.* **228**, 583–592 (1985).
33. Kettle, A. J. & Winterbourn, C. C. A kinetic analysis of the catalase activity of myeloperoxidase. *Biochemistry* **40**, 10204–10212 (2001).
34. Guerin, I. & de Chastellier, C. Pathogenic mycobacteria disrupt the macrophage actin filament network. *Infect. Immun.* **68**, 2655–2662 (2000).
35. Henderson, L. M. & Meech, R. W. Evidence that the product of the human X-linked CGD gene, gp91-phox, is a voltage-gated H⁺ pathway. *J. Gen. Physiol.* **114**, 771–786 (1999).
36. Maturana, A. *et al.* Heme histidine ligands within gp91^{phox} modulate proton conduction by the phagocyte NADPH oxidase. *J. Biol. Chem.* **276**, 30277–30284 (2001).
37. Nanda, A., Romanek, R., Curnutte, J. T. & Grinstein, S. Assessment of the contribution of the cytochrome b moiety of the NADPH oxidase to the transmembrane H⁺ conductance of leukocytes. *J. Biol. Chem.* **269**, 27280–27285 (1994).
38. De Coursey, T. E., Cherny, V. V., Morgan, D., Katz, B. Z. & Dinauer, M. C. The gp91^{phox} component of NADPH oxidase is not the voltage-gated proton channel in phagocytes, but it helps. *J. Biol. Chem.* **276**, 36063–36066 (2001).
39. McCord, J. M. & Wong, K. in *Oxygen Free Radicals and Tissue Damage* (ed. Fitzsimons, D. W.) 343–360 (Excerpta Medica, Amsterdam, 1979).
40. Klebanoff, S. J. & Pincus, S. H. Hydrogen peroxide utilization in myeloperoxidase-deficient leukocytes: a possible microbicidal control mechanism. *J. Clin. Invest.* **50**, 2226–2229 (1971).
41. Brennan, M. L. *et al.* Increased atherosclerosis in myeloperoxidase-deficient mice. *J. Clin. Invest.* **107**, 419–430 (2001).
42. Klebanoff, S. J. & Clark, R. A. Iodination by human polymorphonuclear leukocytes: a re-evaluation. *J. Lab. Clin. Med.* **89**, 675–686 (1977).
43. Grogan, A. *et al.* Cytosolic phox proteins interact with and regulate the assembly of coronin in neutrophils. *J. Cell Sci.* **110**, 3071–3081 (1997).
44. Hall, T. A. & Gupta, B. L. in *Principles of Analytical Electron Microscopy* (eds Joy, D. C., Romig, A. D. & Goldstein, J. I.) 219–248 (Plenum, London, 1986).
45. Olsen, R. L. & Little, C. Purification and some properties of myeloperoxidase and eosinophil peroxidase from human blood. *Biochem. J.* **209**, 781–787 (1983).
46. Sadir, R., Baleux, F., Grosdidier, A., Imberty, A. & Lortat-Jacob, H. Characterization of the stromal cell-derived factor-1- α -heparin complex. *J. Biol. Chem.* **276**, 8288–8296 (2001).
47. Vita, F. *et al.* Preparation of membrane fractions from human neutrophil granules: A simple method. *Methods Cell Sci.* **19**, 197–205 (1997).
48. Barrett, A. J. Cathepsin G. *Methods Enzymol.* **80C**, 561–565 (1981).
49. Amos, B. J., Pocock, G. & Richards, C. D. On the role of bicarbonate as a hydrogen ion buffer in rat CNS neurones. *Exp. Physiol.* **81**, 623–632 (1996).

Supplementary Information accompanies the paper on Nature's website (<http://www.nature.com>).

Acknowledgements

We thank W. Gratzler, P. Rich, F. Ashcroft, M. Brand, R. Vaughan-Jones and M. Duchon for discussions; E. Hawe for statistical analysis; A. Hankin and E. C. Davis for technical assistance; and A. Scott for illustration and art work. The Wellcome Trust and Chronic Granulomatous Disease Research Trust provided financial support.

Competing interests statement

The authors declare that they have no competing financial interests.

Correspondence and requests for materials should be addressed to A.W.S. (e-mail: rmhaase@ucl.ac.uk).